

A compact dual atom interferometer gyroscope based on laser-cooled rubidium

T. Müller,* M. Gilowski, M. Zaiser, T. Wendrich, W. Ertmer, and E. M. Rasel

Institut für Quantenoptik, Leibniz Universität Hannover, Welfengarten 1, 30167 Hannover, Germany

We present a compact and transportable inertial sensor for precision sensing of rotations and accelerations. The sensor consists of a dual Mach-Zehnder-type atom interferometer operated with laser-cooled ^{87}Rb . Raman processes are employed to coherently manipulate the matter waves. We describe and characterize the experimental apparatus. A method for passing from a compact geometry to an extended interferometer with three independent atom-light interaction zones is proposed and investigated. The extended geometry will enhance the sensitivity by more than two orders of magnitude which is necessary to achieve sensitivities better than 10^{-8} rad/s/ $\sqrt{\text{Hz}}$.

PACS numbers: 03.75.Dg, 37.25.+k, 06.30.Gv

I. INTRODUCTION

During the last years, atom interferometry has become an outstanding technique for precision measurements of fundamental constants [1, 2] or inertial forces like accelerations [3] or rotations [4]. Thanks to the progress in quantum engineering of cold atoms, the ultimate potential of matter wave interferometers is still an open question [5], and new atom interferometers aiming for unprecedented sensitivity to be used for improved tests of the fundamental laws of physics on ground [6] or in microgravity environment [7, 8, 9] are an exciting focus of current research. Other activities concern the realization of atomic quantum sensors employed in metrology or in applied sciences. Fields of applications are the monitoring of variations of the geopotential or the earth's rotation [10]. Today, variations of the earth's rotation are measured globally by Very Long Baseline Interferometry (VLBI) [11] or locally with large optical ring laser gyroscopes [12]. Optical gyroscopes massively gain in sensitivity by enlarging the enclosed area up to hundreds of square meters.

In this paper, we present a novel dual atom interferometer for exploring the potential of cold atoms for miniaturized and stable high resolution rotation sensors. The sensor is based on a Mach-Zehnder-type interferometer, where cold atoms are coherently split, redirected and recombined to interfere by velocity-selective Raman transitions. Coherent manipulation by Raman processes was formerly used for atomic gyroscopes using thermal beams [4] or laser-cooled atoms [13]. Our apparatus aims to combine some of the advantages of the two aforementioned experiments. On the one hand, the source system employed for our sensor generates a high effective atomic flux comparable to thermal beams [14]. Moreover, the sensor is based on spatially separated beam splitters for long baseline interferometry allowing to strive for a rotational sensitivity of a few nrad/s/ $\sqrt{\text{Hz}}$. On the other

hand, we employ laser-cooled atoms started in a molasses, thus permitting a precise control of the launch parameters [13] and allowing for a well-defined enclosed area in the interferometer. Additionally, it is anticipated to increase the long-term stability of the rotation measurement by employing compact gyroscopes with laser-cooled atoms to achieve resolutions comparable to [4]. This allows for a highly transportable sensor for comparison campaigns with other state-of-the-art optical and atomic gyroscopes.

In the description of our novel design of an atomic gyroscope using ultra-cold rubidium atoms, we briefly sketch the measurement scheme and then describe the experimental implementation of the interferometer's key elements and their performance. Finally, we present elements and techniques for atom-interferometric in situ diagnostics for such an inertial sensor. In particular, we propose and investigate a method to pass from a single laser beam interferometer to a long baseline design.

II. MACH-ZEHNDER INTERFEROMETRY BASED ON STIMULATED RAMAN TRANSITIONS FOR PRECISION INERTIAL SENSING

The principle of the coherent manipulation of atoms by a two-photon Raman process is described in detail in Ref. [15]. In the Raman process, two long-lived hyperfine states $|g\rangle$ and $|e\rangle$ are coupled by two light fields via an intermediate state $|i\rangle$ which is off-resonance from the single photon excitations.

A Mach-Zehnder-type atom interferometer can be implemented with three such Raman processes separated in time and/or space. The first one coherently transfers the atoms initially prepared in one of the two hyperfine states into a coherent superposition of $|g\rangle$ and $|e\rangle$. Furthermore, this so-called $\pi/2$ -pulse generates two spatially separating matter wave modes, when the two light fields are counterpropagating, similar to a 50/50 beam splitter in optics. The second Raman process, a π -pulse, flips the internal state and the relative momentum of both matter waves and thus acts like a mirror. Recombination of the two matter wave modes is achieved by the third Raman

*Present address: Nanyang Technological University, 1 Nanyang Walk, Block 5 Level 3, Singapore 637616, Singapore

process acting as a coherent beam splitter mixing the two matter wave modes, similar to the first $\pi/2$ -pulse.

In the ideal case, this type of interferometer has two output ports labelled by the internal states $|g\rangle$ and $|e\rangle$ and different momenta. A varying phase difference between the matter wave modes leads to a varying population difference between the two atomic states which is measured by state-selective fluorescence detection. This means that the transition probability $P_{|e\rangle} = N_{|e\rangle}/(N_{|g\rangle} + N_{|e\rangle})$ of populating the excited state [28] depends on the relative phase $\Delta\phi_p$ of both matter wave modes and the relative phase $\Delta\phi_L$ of the light fields between the first and the second, and between the second and the third Raman process:

$$P_{|e\rangle} = \frac{1}{2}(1 + C \cos(\Delta\phi_L + \Delta\phi_p)). \quad (1)$$

Here, C is the contrast of the interferometer and $\Delta\phi_L = \phi_1 - 2\phi_2 + \phi_3$ is the combined phase resulting in the interferometer by the interaction of the atom dipole with the i -th Raman beam splitting pulse ($i = 1, 2, 3$).

Due to its symmetry, the Mach-Zehnder topology is especially suited for the measurement of inertial forces. In the ideal case, the phase difference $\Delta\phi_p$ depends only on the relative motion of the atoms with respect to the light fields driving the Raman process. This relative motion is modified by inertial forces, i.e. rotations and accelerations such that $\Delta\phi_p = \Delta\phi_{\text{rot}} + \Delta\phi_{\text{acc}}$.

The phase shift induced by rotations

$$\Delta\phi_{\text{rot}} = \frac{2m}{\hbar}\vec{\Omega} \cdot \vec{A} \quad (2)$$

depends on the orientation and size of the area \vec{A} enclosed by the interferometer, the rotation vector $\vec{\Omega}$, the mass m of the particle, and Planck's constant \hbar . In an atom interferometer, this phase shift is a factor $mc^2/\hbar\omega \sim 10^{10}$ bigger than in an optical interferometer, assuming the wavelength of visible light and the rubidium mass, as well as an identical enclosed area. This reveals the high potential of matter wave interferometers as an alternative to gyroscopes solely based on light waves, despite the significantly smaller signal-to-noise-ratio (SNR) and enclosed area.

An acceleration \vec{a} of the freely propagating atoms relative to the beam splitting light pulses of the interferometer induces a phase shift given by

$$\Delta\phi_{\text{acc}} = \vec{k}_{\text{eff}}\vec{a}T^2, \quad (3)$$

where \vec{k}_{eff} is the effective wave vector of the Raman laser beams and T the time interval between the different beam splitting pulses.

Employing a Mach-Zehnder interferometer as an inertial sensor requires a distinction between rotations and accelerations. In order to achieve this, we operate the interferometer simultaneously with two atomic sources injecting atoms with opposing velocity direction from opposite sides into the interferometer, as displayed in

Fig. 1. This results in a dual interferometer with two equal, but opposite enclosed areas $\vec{A}_1 = -\vec{A}_2$ [4]. The sign of the phase shift induced by rotations therefore differs between the two interferometers, whereas the phase shift due to accelerations is of equal sign, see Eq. (2) and (3). Consequently, subtraction or addition of the two interferometer signals allows for a discrimination between the two inertial forces. Additionally, common-mode phase noise of the two interferometers, for example induced by the Raman laser beams $\partial\phi_i$, is suppressed by 40 dB due to the utilized differential measurement scheme [16]. The concept of dual atom interferometry has already been successfully implemented in two other atomic gyroscopes [4, 13].

III. EXPERIMENTAL IMPLEMENTATION OF ATOM-OPTICAL ELEMENTS

In this section, we describe the experimental apparatus of our atomic Sagnac interferometer comprising the atomic sources, the laser system for the incoherent and coherent manipulation of the atoms, as well as the state preparation and detection.

A. The main apparatus

The differential measurement scheme of the atomic Sagnac interferometer is reflected by the symmetric design of the main experimental apparatus shown in Fig. 1. It consists of two identical atomic sources [14] generating counterpropagating pulsed or continuous beams of cold atoms injected from two opposite sides into the central part, where the state preparation, the coherent manipulation, and the detection of the atoms is performed. The vacuum system for the generation and manipulation of cold atoms is based on custom-designed aluminum chambers evacuated by a 201/s ion pump and a titanium sublimation pump. The main apparatus with an overall length of only 90 cm is placed on a non-magnetic optical breadboard with a size of $120 \times 90 \text{ cm}^2$. The laser beams for manipulating the atoms are brought to the experiment via polarization maintaining (PM) optical fibers, thus decoupling the laser system from the main apparatus and improving the steady reproducibility of the atom-light interaction. The main experimental apparatus is surrounded by a permalloy magnetic shield to suppress stray fields, and will be put on an active vibration isolation in a later stage to reduce the accelerational noise from the laboratory environment.

B. The atomic sources

The two identical atomic sources will be described only briefly here, as an extensive description and characterization can be found in Ref. [14]. The atomic sources

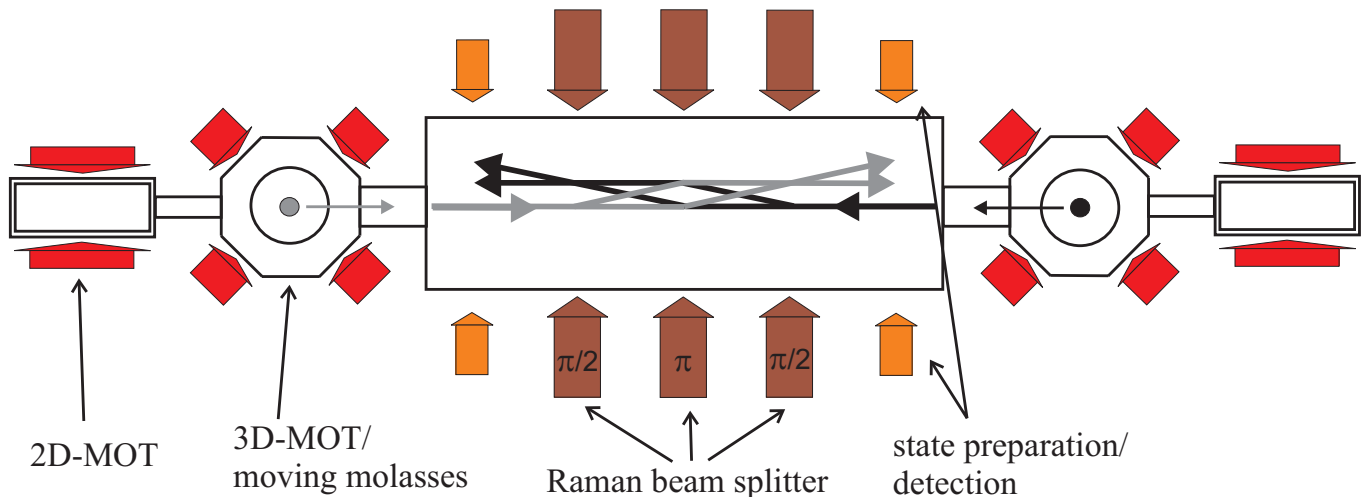


FIG. 1: (color online). Schematic of the dual atom interferometer in top view. The central part shows the interferometry chamber with three spatially separated atom-light interaction zones. Dual stage atom sources for the preparation of the cold atomic ensembles are mounted on both sides of this chamber.

consist of a two-dimensional magneto-optical trap (2D-MOT) loading a subsequent 3D-MOT for pulsed operation of the interferometer. With the 2D-MOT, we obtain a high loading flux of more than 5×10^9 atoms/s into the 3D-MOT. This allows for short loading times of the 3D-MOT compared to the measurement time while still providing atom numbers sufficient to reach a desirable SNR (10^8 atoms in 20 ms loading time).

After loading, the 3D-MOT is switched to a moving molasses configuration [17] launching the atoms into the central interferometer chamber on flat parabolic trajectories. Forward drift velocity and vertical velocity can be tuned independently between 2.5 – 5 m/s and 0 – 1 m/s, respectively, with a relative uncertainty of $< 3 \times 10^{-4}$ to realize perfectly symmetric parabolic trajectories and an optimal spatial overlap of both interferometers. This permits systematic studies and optimization of the interferometer sequence with respect to the suppression of frequency-dependent noise.

Using this technique, the launched atoms, typically started with a forward velocity of 4.4 m/s, reach a temperature of 8 μ K. The precise control of the atomic velocity results in an accuracy of the enclosed interferometer area sufficient for reaching resolutions of rotation rates on the order of a few nrad/s with the completed gyroscope [14].

C. Manipulation of atoms with laser light

Six diode laser systems are used for the manipulation of the ^{87}Rb atoms with light. These are set up together with further optical elements for frequency stabilization and beam manipulation on two $60 \times 90 \text{ cm}^2$ optical breadboards. Cooling and trapping of the atoms is performed with two commercial high-power diode laser systems

locked close to the $|F = 2\rangle \rightarrow |F' = 3\rangle$ cooling transition. The light for repumping atoms from $|F = 1\rangle$ to $|F = 2\rangle$ via optical pumping from $|F = 1\rangle \rightarrow |F' = 2\rangle$, for fluorescence detection by driving the transition $|F = 2\rangle \rightarrow |F' = 3\rangle$, as well as for the state preparation addressing the transition $|F = 2\rangle \rightarrow |F' = 2\rangle$ is realized with self-made external cavity diode lasers (ECDL) [18].

State preparation and detection

The two atomic states used for interferometry are the magnetically insensitive $m_F = 0$ -Zeeman states of the hyperfine ground states $|F = 1\rangle$ and $|F = 2\rangle$ of ^{87}Rb . After the launch, the atoms populating all m_F -substates of $|F = 2\rangle$ are spin-polarized into the $|F = 1, m_F = 0\rangle$ state by the following procedure: We apply a 0.4 ms long π -polarized light pulse resonant with the $|F = 2\rangle \rightarrow |F' = 2\rangle$ transition. The atoms are thus optically pumped into the $|F = 2, m_F = 0\rangle$ ground state which decouples from the light due to optical selection rules. During optical pumping, we simultaneously repump atoms decayed into the $|F = 1\rangle$ state by addressing the $|F = 1\rangle \rightarrow |F' = 2\rangle$ transition. The repumping light is maintained 0.4 ms longer than the pumping light to completely depopulate the lower hyperfine level. The optical pump is followed by a resonant π -pulse with the Raman lasers at a frequency difference of about 6.834 GHz to transfer the atoms from the $|F = 2, m_F = 0\rangle$ state into the $|F = 1, m_F = 0\rangle$ state. The atoms remaining in the $|F = 2\rangle$ -manifold after the π -pulse are removed by the light pressure from a σ^+ -polarized light pulse tuned in resonance with the closed transition $|F = 2\rangle \rightarrow |F' = 3\rangle$. The spin polarization of this preparation scheme is better than 99.9%. The optical pumping leads to a slight heating of the atomic sample to about 10 μ K. In the upgraded version of our Sagnac interferometer, we plan to

combine the internal state selection with a velocity filter by employing velocity-selective Raman processes [19].

The detection of the relative atom number $N_{|e\rangle}/(N_{|g\rangle} + N_{|e\rangle})$ is performed in a sequence similar to the fluorescence detection schemes used in atomic fountain clocks [20], where our sequence is pulsed in time rather than in space. In the first step, we determine the number $N_{|e\rangle}$ of atoms in the state $|e\rangle = |F = 2, m_F = 0\rangle$ by applying a 0.8 ms long nearly resonant detection pulse at a detuning of $\delta = 5$ MHz on the closed transition $|F = 2\rangle \rightarrow |F = 3\rangle$. The light beam with an intensity of I_{sat} [29] is σ^+ -polarized and retro-reflected to avoid loss of atoms. The induced fluorescence is recorded on a calibrated photo diode collecting about 1.8% of the isotropically scattered light. This detection step is followed by a 0.4 ms long repumping pulse on the transition $|F = 1\rangle \rightarrow |F' = 2\rangle$, thus bringing all the atoms into the upper hyperfine ground state. In the last step, we repeat the first detection light pulse and by using the same photo diode we determine the absolute number of atoms $N_{|g\rangle} + N_{|e\rangle}$. We currently reach a SNR of 30 with the described detection scheme which is mainly limited by the frequency noise of the detection laser.

Coherent beam splitting with Raman processes

The interferometer's light pulse sequence is performed by two digitally phase-locked Raman lasers driving the hyperfine transition at $\omega_{\text{eff}} = \omega_1 - \omega_2 \approx 6.834$ GHz. The two lasers are tuned off-resonance from the transitions $|F = 1\rangle \rightarrow |F' = 1\rangle$ and $|F = 2\rangle \rightarrow |F' = 1\rangle$ by the variable detuning of $\Delta = 0.4 - 3$ GHz.

The two self-made high-power diode laser systems [21] have a total laser power of 700 and 500 mW, respectively. This is sufficient to reach pulse lengths of as short as several μs for the realization of the interferometer pulses (at a detuning Δ of 1 GHz), even for the rather large diameters of 30 mm used for the Raman beam splitters. This pulse length has been inferred to be optimal with respect to the matching of the Doppler-broadened transition with the Fourier-limited excitation profile of the Raman transition, as well as with respect to the influence of frequency dependent noise sources in our interferometer [22].

The phase difference of the two lasers is tightly locked with an optical phase-locked loop (PLL) [23]. This is achieved by monitoring the beat note of the two light fields and comparing the beat frequency and phase difference with a high-quality crystal oscillator. Our system realizing the PLL is almost identical to the one described in [22]. We specify the rms phase error in each of the interferometers caused by the phase noise of the Raman laser system to be about 1 mrad without common-mode noise suppression. This estimation is based on the residual phase noise of the Raman laser system and the weighting function of our upgraded interferometer, where the weighting function is a measure for the influence of frequency dependent noise sources on the interferome-

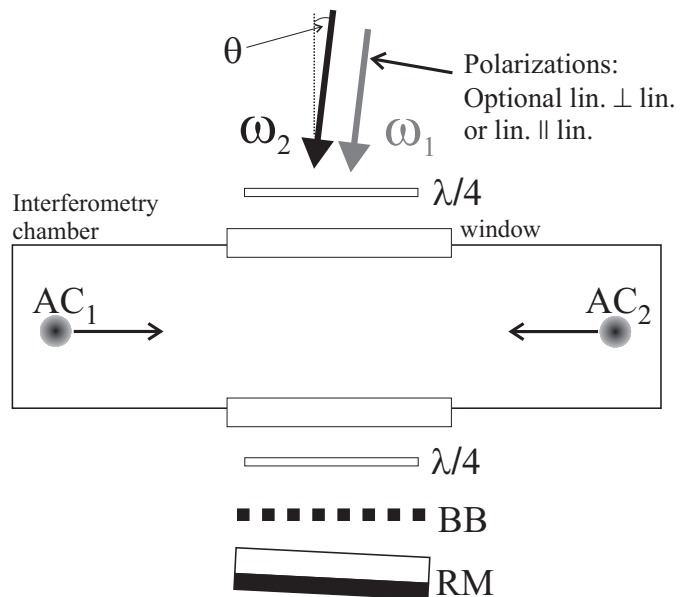


FIG. 2: Schematic of the optical realization of the Raman beam splitters. The two atomic clouds ($AC_{1,2}$) are coherently manipulated by inducing Raman transitions with the two laser beams of frequency ω_1 and ω_2 . The transition can be induced with equal circular ($\sigma^+ - \sigma^+$ or $\sigma^- - \sigma^-$) or crossed linear polarization of the two lasers. This is used to choose the velocity-selectivity of the transition by changing the polarization of the incoming Raman beams. For velocity-unselective transitions, the beams are absorbed by a beam block (BB) after crossing the atom-light interaction zone once, while for velocity-selective transitions they cross the interaction zone twice by using a retro-reflecting mirror (RM).

ter's performance. The interferometer experiences different sensitivities to phase noise during one experimental cycle, for example the loading time of the MOT (no sensitivity) compared to the time between the beam splitting pulses (highest sensitivity).

Both beams are guided to the atom-light interaction zone in the same PM optical fibre with either identical or crossed linear polarization for velocity-unselective or velocity-selective Raman transitions, respectively. A schematic of the optical realization of the velocity-unselective and velocity-selective Raman beam splitters, respectively, is depicted in Fig. 2. To drive velocity-unselective transitions, the two beams are blocked after passing the interferometer once. To implement velocity-selective transitions, the two beams pass a $\lambda/4$ -wave plate before and after the atom-light interaction zone and are then retro-reflected to pass the wave plates and the interaction zone a second time. In this configuration, only velocity-selective Raman transitions with opposing laser beam directions are possible due to optical selection rules. By aligning the laser beams with a small angle offset of $\theta \approx 12$ mrad from perpendicular incidence with respect to the atomic trajectories, a small Doppler shift can be introduced in the velocity-selective Raman transition. Thus, one of the (otherwise degenerate) Raman

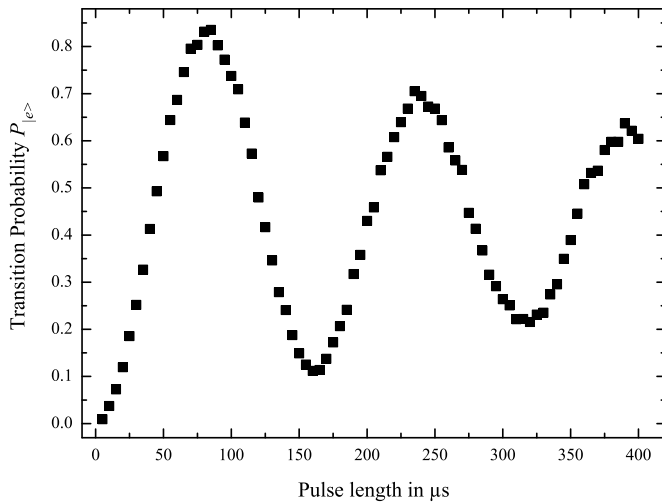


FIG. 3: Rabi oscillations between the two atomic states used in the interferometer induced by velocity-unselective Raman transitions. The oscillations are observed by varying the pulse length of the Raman transition.

transitions induced by the two pairs of counterpropagating laser beam pairs ($\sigma^+ - \sigma^+$ or $\sigma^- - \sigma^-$) can be selected by compensating the corresponding Doppler detuning by the frequency difference ω_{eff} of the Raman laser beams. While in the first case of velocity-unselective Raman transitions only the photon recoil corresponding to the microwave frequency ω_{eff} is transferred to the atoms, velocity-selective Raman transitions will lead to a momentum transfer of roughly twice the recoil of the optical photon.

For the studies presented in this paper, we used a Raman atom interferometer with an effective length of about 9 mm, corresponding to a total interferometer time of $2T = 2$ ms. The co- or counterpropagating pair of Raman laser beams is pulsed onto the atoms, while these cross the Gaussian laser beam profile in the center of the interferometer chamber. The large beam diameter, as well as optics with a specified distortion of less than $\lambda/20$ assure a sufficient quality of the wave front.

IV. ATOM-INTERFEROMETRIC IN SITU DIAGNOSTICS FOR INERTIAL SENSING

Characterization and optimization of the atom interferometer is an iterative process of various in situ measurements. The flexibility of the Raman process with respect to the coherent manipulation of the atoms allows for the implementation of a variety of atom-interferometric tools to characterize the performance and systematics of the inertial sensor. This tool box comprises the individual velocity-unselective or -selective Raman process as the simplest element to coherently manipulate the atoms, Ramsey-type experiments to analyze systematics, as well as Mach-Zehnder-type interferome-

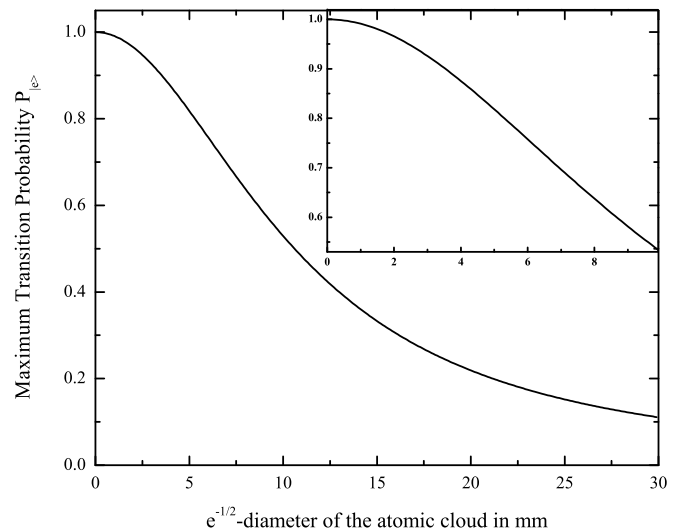


FIG. 4: Maximum population transfer efficiency as a function of the diameter of the atomic cloud.

try to determine the orientation of the setup or ultimately to measure rotation rates.

In the following sections, we describe measurements to evaluate the performance of our sensor including the influence of the atomic temperature and the effective atomic flux Φ_{eff} . The effective atomic flux Φ_{eff} is given by twice the product of the total number $N_{|g\rangle} + N_{|e\rangle}$ of atoms detected per shot, the contrast C of the interferometer, and the cycling rate Γ of the sensor:

$$\Phi_{\text{eff}} = 2(N_{|g\rangle} + N_{|e\rangle})CT. \quad (4)$$

Additionally, we demonstrate tools for proceeding to the finite interferometer geometry to achieve the ultimate sensitivity.

A. Alignment and contrast of the Mach-Zehnder Interferometer

The achievable contrast C of a Raman atom interferometer is limited by the parameters of the atomic cloud, such as its spatial spread in size or its temperature, which have to be compared to the technical parameters of the matter wave beam splitters. These are power, detuning, and diameter of the Raman laser beams determining in combination the length of the $\pi/2$ - and π -pulses. An upper limit for the achievable contrast can be inferred from the performance of the individual Raman processes, i.e. the beam splitting, reflection, and recombination. The characterization of the velocity-unselective Raman process reveals the influence of the width of the atomic cloud spread across the Gaussian intensity profile of the Raman laser beams during the atom-light interaction. This Gaussian intensity profile leads to varying Rabi frequencies for the individual atoms manipulated with the Raman lasers. However, as the length of a beam splitter

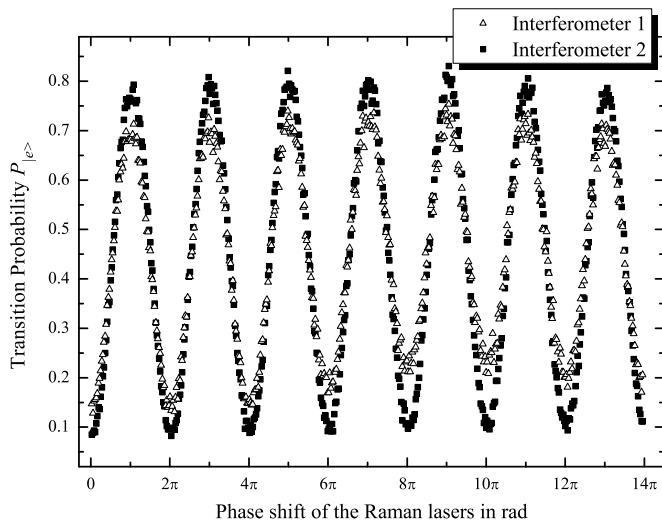


FIG. 5: Interference fringes in the echo-type sequence (Mach-Zehnder-type configuration) for velocity-unselective Raman transitions. To observe the fringes, the phase difference between the two Raman lasers is scanned between the π - and the last $\pi/2$ -pulse of the interferometer sequence. The reduced contrast of interferometer 1 in this particular measurement is caused by a reduced state preparation efficiency due to technical imperfections.

pulse is the same for all atoms, this leads to a decrease in the maximum transition probability being averaged over all atoms. The spatial spread of the atomic ensemble during the different instants of atom-light interaction is a function of the distance to the corresponding atomic source, the drift velocity, the size of the atomic cloud after preparation, and the temperature of the atomic ensemble.

In our setup, the atomic cloud has a $1/\sqrt{e}$ -diameter of 4.4 mm in the middle of the interaction zone which is to be compared to a $1/e^2$ -diameter of the Raman laser beams of 30 mm. This leads to a maximum population transfer efficiency of 85% with a single π -pulse, as shown in Fig. 3. The dependance of the maximum excitation probability, and thus the reflectivity, on the $1/\sqrt{e}$ -diameter of the atomic cloud is displayed in Fig. 4. Further compression of the atomic cloud before the launch [24], a larger diameter of the atom-light interaction zone and more light power can improve the reflectivity to about 95%. We find that even for the longest flight times of the atoms the influence of the expansion of the ensemble due to its temperature is smaller than the initial spatial width.

The synchronization of the Raman pulse with the passing of the atoms through the center of the Gauss-shaped Raman laser beam is optimized in situ by minimizing the duration of a π -pulse by varying the timing of the pulse. Thus, a precise knowledge of the start location of the atoms with respect to the Raman laser beams is not necessary. This method permits to align the $\pi/2 - \pi - \pi/2$ -sequence of the dual interferometer with respect to the

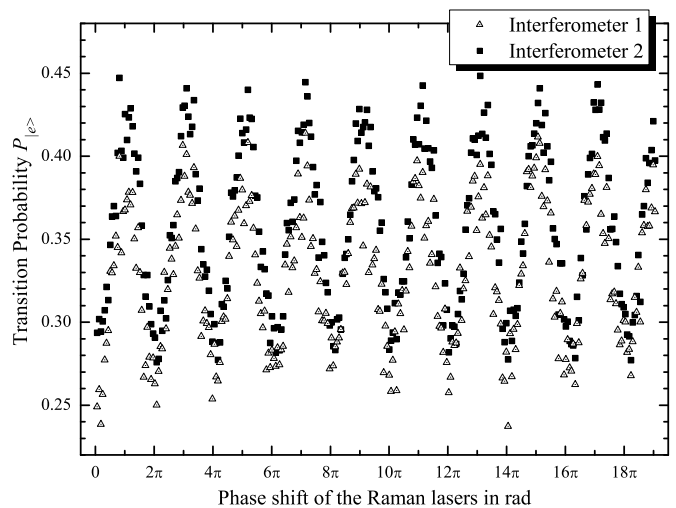


FIG. 6: Interference fringes in the Mach-Zehnder-type configuration for velocity-selective Raman transitions. The oscillations of the transition amplitude are induced as explained in the caption of Fig. 5.

atomic parabolas with perfect symmetry.

Fig. 5 shows a combination of all steps of coherent manipulation to a $\pi/2 - \pi - \pi/2$ -sequence, resulting in a contrast of 72% in our apparatus. The effective atomic flux of the interferometer is 2.2×10^7 atoms/s. The difference in contrast between the two atom interferometers is caused by an imperfect state preparation at the entrance of the interferometers. The measures for improving the reflection efficiency of the π -pulse discussed above would result in a contrast of the interferometer of more than 90% which may even be enhanced by an adaption of the length of the beam splitting pulses, thus compensating the spatially varying Rabi frequency due to the Gaussian intensity profile of the laser beams over the whole interferometer region [25].

As shown in Fig. 6, the atomic temperature, or more precisely the velocity dispersion along the Raman laser beams is much more critical in the case of velocity-selective Raman transitions. Usually, the frequency width of the resonance of the Raman process is Fourier-limited by the pulse duration and is by this means adapted to the atomic temperature. The maximum transition probability amounts to a fraction of 33% of the 10 μ K cold atomic ensemble in our apparatus for the individual velocity-selective Raman process with a pulse duration of as short as 10 μ s. This leads to a theoretical contrast of the inertial sensor of 20%. The observed contrast shown in Fig. 6 is even further reduced due to vibrational noise which has to be shielded by an active noise cancellation in the future. The effective atomic flux in the Mach-Zehnder interferometer is 6×10^6 atoms/s. A contrast close to the velocity-unselective case can in principle be achieved by a further reduction of the atomic temperature down to 1.5 μ K or by adequate velocity filtering [19].

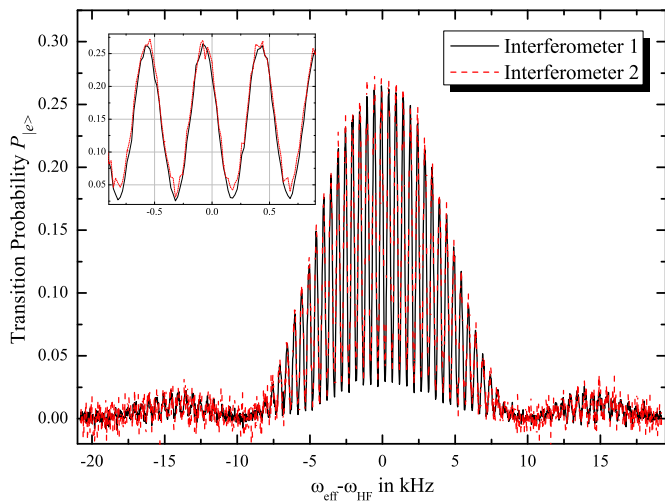


FIG. 7: (color online). Typical interference pattern for the Ramsey-type interferometer. The observed oscillations of the transition amplitude are induced by scanning the frequency difference ω_{eff} between the two lasers driving the Raman transition close to the hyperfine splitting $\omega_{\text{HF}} = 6.8346826$ GHz.

The presented temporal Mach-Zehnder-type interferometer can be used to precisely align the long baseline interferometer perpendicular to local gravity, as well as to optimize the relative orientation of the spatially separated beam splitters with respect to each other. For this procedure, each of the individual Raman sequences has to be replaced by a full temporal Mach-Zehnder sequence. We demonstrated this method in the central viewport of our interferometer chamber. Even for a short total interrogation time of up to $2T = 4$ ms we can obtain a sensitivity of $2 \times 10^{-3} \text{ m/s}^2/\sqrt{\text{Hz}}$ for accelerations and $2 \times 10^{-4} \text{ rad/s}/\sqrt{\text{Hz}}$ for rotations in our dual atom interferometer.

The intrinsic atomic accelerometer can be used to monitor the orientation of our atomic Sagnac sensor with respect to local gravity by combining measurements in the vertical and horizontal direction with a local tide model. Monitoring the earth's rotation rate with a resolution of 10^{-9} rad/s corresponds to a control of the angle between the area normal vector of the atom interferometer and the local direction of gravity to about $1 \mu\text{rad}$.

B. Control and evaluation of systematic effects by Ramsey-type measurements

Besides inertial forces, the Mach-Zehnder interferometer is also sensitive to changes in the applied frequency difference of the Raman lasers from the atomic resonance frequency which can e.g. be perturbed by magnetic or electric fields. Therefore, these effects have to be evaluated systematically to minimize undesired phase shifts caused by frequency-changing effects, such as the Zeeman effect. Contrary to the Ramsey-type measure-

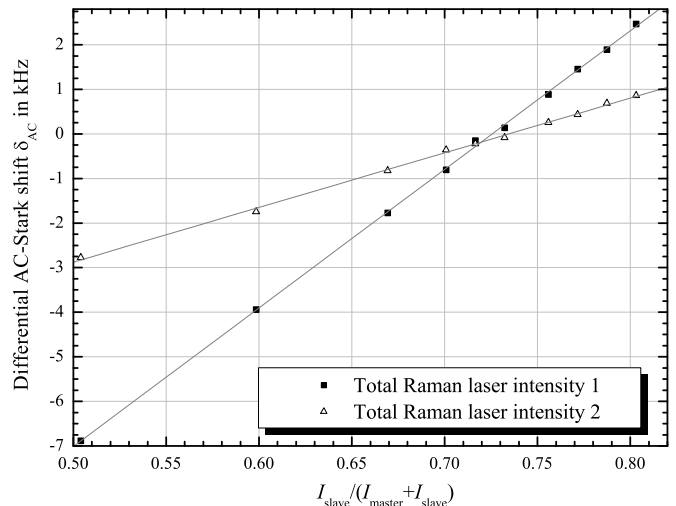


FIG. 8: Measured differential AC-Stark shift δ_{AC} of the atomic resonance as a function of the intensity ratio of the two Raman lasers for constant total laser intensity. The linear dependance of δ_{AC} is shown for two different total Raman laser intensities.

ment employed in atomic clocks, the sensitivity to frequency changes in the Mach-Zehnder interferometer does not scale with the time T between the pulses, but with the length of the pulses τ . We therefore investigate frequency shifts with Ramsey-type interferometry based on velocity-unselective Raman processes. This provides valuable information on the control of systematic shifts and their contribution to the short-term sensitivity of the inertial sensor due to fluctuations of the relevant parameters. The signal of the Ramsey-type interferometer, i.e. the population of the two hyperfine ground states separated by an energy spacing of $\hbar\omega_{\text{HF}}$ is sensitive to shifts of the frequency difference ω_{eff} between the Raman lasers:

$$P_{|e\rangle} \propto (1 + \cos(\omega_{\text{HF}} - \omega_{\text{eff}})T). \quad (5)$$

Here, T is the separation of the two Raman pulses in time which is usually significantly larger than the duration of a single Raman pulse (some ms compared to some $10 \mu\text{s}$). Shifts of the atomic resonance frequency are inferred by the determination of the position of the central interferometer fringe while scanning the frequency difference ω_{eff} between the Raman laser pair across the resonance, as shown in Fig. 7.

We investigated the differential AC-Stark shift, as well as the Zeeman shift with the Ramsey-type configuration. As the single-photon AC-Stark shifts of the two atomic levels depend differently on the intensity of the corresponding Raman laser (I_{master} and I_{slave} , respectively), one can find a ratio of both intensities for which the differential AC-Stark shift cancels [4]. This ratio is determined by varying the individual laser intensities for a fixed total intensity resulting in a linear frequency shift of the resonance, as shown in Fig. 8. With two series of such measurements, we infer the optimum intensity ratio up

to an uncertainty corresponding to a residual AC-Stark shift δ_{AC} of 150 Hz limited by the power stability of the Raman lasers during the measurement cycle. This corresponds to a phase shift of about 13 mrad in our interferometer which should be suppressed in the differential measurement scheme for slowly varying intensities of the Raman lasers.

The interferometer is operated with a small magnetic bias field of typically 400 mG to lift the degeneracy of the m_F -substates and to establish a quantization axis for the spin-polarized ensemble. This necessitates the precise determination of the second order Zeeman effect and possible fluctuations in the magnetic bias field. The Ramsey-type measurements show that the frequency shift due to the quadratic Zeeman effect can be controlled to about ± 1.4 Hz. With this in situ measurement, we determine a reduction of unwanted external magnetic fields in the interferometer to about 10 mG corresponding to a suppression of the earth's magnetic field by the permalloy magnetic shield of at least a factor of 50.

V. CONCLUSION AND OUTLOOK

In this paper, we have presented a novel design of a compact dual atom interferometer for high resolution rotation sensing. The apparatus aims to combine advantages of other state-of-the-art sensors [4, 13], such as high atomic flux equivalent to thermal beams and long baseline interferometry, but with the advantages of cold atoms. We have presented different measurement schemes for in situ analysis and optimization of the dual atom interferometer including the measurement of systematic effects, such as the Zeeman and the AC-Stark shift. We indicated a concept to pass from a temporal sequence with one spatial atom-light interaction zone to long baseline atom interferometry. The measurement of the sensor's inclination with respect to local gravity also permits to align the surface orientation of the sensitive axis of the sensor with the earth's rotation axis with the

required accuracy.

The upgrade of the sensor to a long baseline interferometer will enhance the sensitivity by more than two orders of magnitude compared to the temporal Mach-Zehnder geometry realized so far. The present resolution of phase shifts of 100 mrad is mainly limited by vibrations and technical noise sources of the detection laser. We expect a reduction of this phase uncertainty down to 1 mrad due to several improvements, like a reduction of the detection noise by using novel laser systems [26, 27] with a linewidth two orders of magnitude lower than the previous system used, a reduction of the atomic temperature by a factor of 4, as well as an enhancement of the contrast of the interferometer by a velocity-selective filter for the atoms participating in the Raman process.

By combining all the described measures, a short-term resolution of rotation rates of several nrad/s for one second of measurement time comes into reach. This will be an interesting regime to investigate the potential of differential atom interferometry and the limitations imposed on the suppression of common-mode noise or the stability of the setup. These studies will provide insight on the fundamental limitations of atom interferometers and their potential for miniaturizing today's active ring laser gyroscopes searching for relative variations of the earth's rotation rate of 1 part in 10^7 .

Acknowledgments

We thank Ch. Jentsch for his contributions during the early stage of the experiment, G. Santarelli and D. Chambon for their support regarding the Raman laser system, and F. Pereira Dos Santos for valuable discussions. This work was supported in part by the Deutsche Forschungsgemeinschaft (SFB 407) and in part by the European Union (Contr. No. 012986-2 (NEST), FINAQS). M.G. would like to thank the Max-Planck-Gesellschaft for financial support.

-
- [1] A. Wicht, J. M. Hensley, E. Sarajlic, S. Chu, *Physica Scripta* **T102**, 82 (2002)
 - [2] A. Bertoldi, G. Lamporesi, L. Cacciapuoti, M. de Angelis, M. Fattori, T. Petelski, A. Peters, M. Prevedelli, J. Stuhler, and G. M. Tino, *Eur. Phys. J. D.* **40**, 271 (2006); J. B. Fixler, G. T. Foster, J. M. McGuirk, M. A. Kasevich, *Science* **315**, 74 (2007)
 - [3] A. Peters, K. Y. Chung, S. Chu, *Nature* **400**, 849 (1999)
 - [4] T. L. Gustavson, A. Landragin, M. A. Kasevich, *Class. Quant. Grav.* **17**, 2385 (2000)
 - [5] M. A. Kasevich, *Science* **298**, 1363 (2002)
 - [6] S. Dimopoulos, P.W. Graham, J.M. Hogan, M. A. Kasevich, *Phys. Rev. Lett.* **98**, 111102 (2007)
 - [7] C. Jentsch, T. Müller, E.M. Rasel, W. Ertmer, *Gen. Rel. Grav.* **36**, 2197 (2004)
 - [8] A. Vogel, M. Schmidt, K. Sengstock, K. Bongs, W. Lewoczko, T. Schuldt, A. Peters, T. Van Zoest, W. Ertmer, E. Rasel, T. Steinmetz, J. Reichel, T. Könemann, W. Brinkmann, E. Göklü, C. Lämmerzahl, H. J. Dittus, G. Nandi, W. P. Schleich, R. Walser, *Appl. Phys. B* **84**, 663 (2006)
 - [9] R.A. Nyman, G. Varoquaux, F. Lienhart, D. Chambon, S. Boussen, J. F. Clément, T. Müller, G. Santarelli, F. Pereira Dos Santos, A. Clairon, A. Bresson, A. Landragin, P. Bouyer, *Appl. Phys. B* **84**, 643 (2006)
 - [10] K. U. Schreiber, T. Klügel, G. E. Stedman, *J. Geophys. Res.* **108**, 2132 (2003)
 - [11] W. Schlüter, D. Behrend, *J. Geod.* **81**, 379 (2007)
 - [12] R. W. Dunn, D. E. Shabalin, R. J. Thirkettle, G. J. MacDonald, G. E. Stedman, K. U. Schreiber, *Appl. Opt.* **41**, 1685 (2002)
 - [13] B. Canuel, F. Leduc, D. Holleville, A. Gauguier, J. Fils,

- A. Viridis, A. Clairon, N. Dimarcq, Ch. J. Bordé, A. Landragin, Phys. Rev. Lett. **97**, 010402 (2006)
- [14] T. Müller, T. Wendrich, M. Gilowski, C. Jentsch, E. M. Rasel, W. Ertmer, Phys. Rev. A **76**, 063611 (2007)
- [15] *Atom Interferometry*, edited by P. R. Berman, (Academic press, San Diego, 1997)
- [16] B. Canuel, *Étude d'un gyromètre à atomes froids*, PhD Thesis, Laboratoire National de Métrologie et d'Essai-SYRTE (2007)
- [17] C. Salomon, J. Dalibard, W. D. Phillips, A. Clairon, S. Guellati, Atomic Phys. **12**, ed. R. Lewis, J. C. Zorn, 73 (1991)
- [18] L. Ricci, M. Weidemüller, T. Esslinger, A. Hemmerich, C. Zimmermann, V. Vuletic, W. König, T.W. Hänsch, Opt. Comm. **117**, 541 (1995)
- [19] M. Kasevich, D. S. Weiss, E. Riis, K. Moler, S. Kasapi, S. Chu, Phys. Rev. Lett. **66**, 2297 (1991)
- [20] S. Bize, Y. Sortais, M. S. Santos, C. Mandache, A. Clairon, C. Salomon, Europhys. Lett. **45**, 558 (1999)
- [21] A. C. Wilson, J. C. Sharpe, C. R. McKenzie, P. J. Manson, D. M. Warrington, Appl. Opt. **37**, 4871 (1998); D. Voigt, E. C. Schilder, R. J. C. Spreeuw, H. B. v. Linden v. d. Heuvell, Appl. Phys. B **72**, 279 (2001)
- [22] P. Cheinet, B. Canuel, F. Pereira dos Santos, A. Gauguet, F. Yver-Leduc, A. Landragin, IEEE Trans. Instrum. Meas. **57**, 1141 (2008)
- [23] G. Santarelli, A. Clairon, S. N. Lea, G. M. Tino, Opt. Comm. **104**, 339 (1994)
- [24] W. Petrich, M. H. Anderson, J. R. Ensher, E. A. Cornell, J. Opt. Soc. Am. B **11**, 1332 (1994); M. T. DePue, S. L. Winoto, D. J. Han, D. S. Weiss, Opt. Comm. **180**, 73 (2000)
- [25] M. Gilowski, T. Wendrich, T. Müller, Ch. Jentsch, W. Ertmer, E. M. Rasel, W. P. Schleich, Phys. Rev. Lett. **100**, 030201 (2008)
- [26] X. Baillard, A. Gauguet, S. Bize, P. Lemonde, Ph. Laurent, A. Clairon, P. Rosenbusch, Opt. Comm. **266**, 609 (2006)
- [27] M. Gilowski, Ch. Schubert, M. Zaiser, W. Herr, T. Wübbena, T. Wendrich, T. Müller, E. M. Rasel, W. Ertmer, Opt. Comm. **280**, 443 (2007)
- [28] $N_{|g\rangle}$ and $N_{|e\rangle}$ denote the number of atoms in the corresponding state.
- [29] $I_{\text{sat}}=1.669(2)$ mW/cm² denotes the saturation intensity.